Energy Conversion and Management 89 (2015) 833–842

Contents lists available at ScienceDirect

Energy Conversion and Management

journal homepage: www.elsevier.com/locate/enconman

Numerical study of finned heat pipe-assisted thermal energy storage system with high temperature phase change material

Saeed Tiari, Songgang Qiu *, Mahboobe Mahdavi

Department of Mechanical Engineering, Temple University, 1947 N. 12th Street, Philadelphia, PA 19122, USA

ARTICLE INFO

Article history:
Received 2 September 2014
Accepted 24 October 2014
Available online 13 November 2014

Keywords:
Latent heat
Thermal energy storage
Heat pipe
Fins
Natural convection
High temperature phase change material

ABSTRACT

In the present study, the thermal characteristics of a finned heat pipe-assisted latent heat thermal energy storage system are investigated numerically. A transient two-dimensional finite volume based model employing enthalpy-porosity technique is implemented to analyze the performance of a thermal energy storage unit with square container and high melting temperature phase change material. The effects of heat pipe spacing, fin length and numbers and the influence of natural convection on the thermal response of the thermal energy storage unit have been studied. The obtained results reveal that the natural convection has considerable effect on the melting process of the phase change material. Increasing the number of heat pipes (decreasing the heat pipe spacing) leads to the increase of melting rate and the decrease of base wall temperature. Also, the increase of fin length results in the decrease of temperature difference within the phase change material in the container, providing more uniform temperature distribution. It was also shown that number of the fins does not have a significant effect on the performance of the system.

1. Introduction

One of the main concerns associated with most of the solar power systems is the continuous power production during cloud transients and non-daylight hours. Thermal energy storage (TES) systems provide a good solution to this issue. Latent heat thermal energy storage (LHTES) systems offer the possibility of storing higher amounts of energy per unit of storage material mass in comparison to sensible heat thermal energy storage (SHTES) systems. However, the performance of most commercially viable phase change materials (PCMs) which used as storage media in the LHTES systems suffer from low thermal conductivity. This often leads to much longer charging or discharging process and significant temperature difference within PCM, which in some cases can cause system overheating and material failure.

Due to the broad applications of LHTES systems in different areas such as solar systems [1,2], electronic cooling [3–5], building heating and hot water [6–8], drying equipment [9,10], air conditioning [11], refrigeration [12] and waste heat recovery [13], various approaches have been developed to resolve the main drawback of LHTES systems, low thermal conductivity of PCM. The example of commonly used methods include the dispersion of high conductivity particles in the PCM [14–17], embedding the PCM in the high conductivity porous medium [18–24] as well as inserting extended surfaces and fins [25–28].

Another popular technique to improve heat transfer to and from PCM is by utilizing heat pipe (HP). HP is capable of transferring large quantities of heat through a small cross-sectional area over a relatively long distance with an extremely small temperature drop [29].

A number of experimental and numerical studies have been conducted to investigate the effects of employing heat pipes to aid PCM melting and solidification in LHTES systems. Majority of these studies were focused on the utilization of low melting temperature PCMs, such as paraffin wax [30–33]. Liu et al. [32,33] experimentally studied a paraffin (T_m = 52.1 °C) based LHTES equipped with heat pipe heat exchanger. They investigated the effects of heat transfer fluid (HTF) inlet temperature and flow rate on the charging only, discharging only and simultaneous charging/discharging process of the system. In another low melting temperature PCM–LHTES analysis, Robak et al. [34] compared the performance of a HP-assisted LHTES to a system utilizing fins in lieu of HPs and a system with neither HPs nor fins. The results indicated that employing HPs makes considerable improvement in both melting and solidification rates. Sharifi et al. [35] investigated the melting and solidification of n-Octadecane (T_m = 28 °C) using heat

* Corresponding author. Tel.: +1 215 204 8530; fax: +1 215 204 4956.
E-mail addresses: saeed.tiari@temple.edu (S. Tiari), songgang.qiu@temple.edu (S. Qiu), mahboobe.mahdavi@temple.edu (M. Mahdavi).

http://dx.doi.org/10.1016/j.enconman.2014.10.053
0196-8904/

Nomenclature

Latin

A_{mush}	mushy zone constant
c_p	specific heat, J kg^{-1} K^{-1}
f_l	liquid fraction
g	gravitational acceleration, m s^{-2}
h	sensible enthalpy, kJ kg^{-1}
h_{sl}	latent heat of fusion, kJ kg^{-1}
H	enthalpy, kJ kg^{-1}
k	thermal conductivity, W m^{-1} K^{-1}
L	length, m
N	number of fins
N_x	number of elements in x-direction
N_y	number of elements in y-direction
P	pressure, Pa
q	heat flux, W m^{-2}
S	spacing, m
t	thickness, m
T	temperature, K
u, v	velocity components, m s^{-1}
x, y	cartesian coordinates

Greek

β	thermal expansion coefficient, K^{-1}
ΔH	latent heat, kJ kg^{-1}
$\Delta\tau_1$	time step before melting, s
$\Delta\tau_2$	time step after melting, s
μ	dynamic viscosity, kg m^{-1} s^{-1}
ρ	density, kg m^{-3}
τ	time, s

Subscripts

eff	effective
f	fin
hp	heat pipe
m	melting
p	pull
r	receiver
ref	reference value
x	component of x direction
y	component of y direction

pipe-metal foil approach experimentally and numerically. It was reported that the integration of heat pipe with metal foil improved the melting and solidification rates significantly.

It should be noticed that the LHTES units incorporated in concentrated solar power (CSP) systems require high melting temperature PCMs to provide high system efficiency. In DOE SunShot program mission statement, it is of great importance to reach Levelized Cost of Energy (LCOE) target of 6 cents per kilowatt hour for the CSP systems to be competitive. It is stated that the best way to achieve the target LCOE is to increase the system efficiency via high operating temperature [36]. However, a very few studies have been dedicated to this area.

In one of scarce experimental efforts with high melting temperature PCM, Qiu et al. [37] investigated a heat pipe-assisted LHTES system coupled with a free piston Stirling engine based CSP. The TES system consisted of a primary heat pipe, an array of 32 secondary heat pipes and PCM which was a eutectic blend of sodium fluoride (NaF) and sodium chloride (NaCl) with melting temperature of 680 °C. The melting temperature of this PCM mixture was chosen to be the same as the Stirling engine operating temperature for optimal CSP performance. The effect of TES orientation on system performance during charging and discharging modes was studied.

A series of thermal resistance network models have been developed to investigate LHTES systems with PCMs such as potassium nitrate (KNO_3, T_m = 335 °C). Shabgard et al. [38] presented a thermal resistance network model to study the influence of inserting multiple heat pipes between heat transfer fluid (HTF) and PCM. Two different configurations were considered in both charging and discharging processes to study the impact of number of HPs as well as their orientation relative to the flow direction on the thermal behavior of HP-assisted LHTES system. Nithyanandam and Pitchumani [39] developed a similar thermal resistance network model with a quasi-steady approach to evaluate the performance of the system during charging and discharging. The effects of heat pipe and LHTES geometric parameters on the transient thermal response of the system were assessed. In another analytical modeling, Jung and Boo [40] predicted the temporal thermal behavior of a finned heat pipe-assisted LHTES system under pure conduction without considering natural convection in molten PCM. The effects of fin pitch on different thermal characteristics of the system such as the heat transfer rate and the transient temperature variations were studied.

The discharging process of a LHTES system was studied numerically by Gou and Zhang [41] using a eutectic mixture of potassium nitrate (KNO_3) and sodium nitrate ($NaNO_3$) with melting temperature of 220 °C as PCM. They employed a transient two-dimensional model without considering natural convection to investigate the effects of utilizing aluminum foils in the PCM as a heat transfer enhancement approach. The results demonstrated that adding aluminum foils accelerated the system discharging process remarkably. Okello et al. [42] studied the combination of rock particle and PCM for high temperature thermal energy storage experimentally. The PCM used in their study was a eutectic mixture of sodium nitrate ($NaNO_3$) and potassium nitrate (KNO_3), the same PCM used by Gou and Zhang [41]. It was shown that embedding PCM cylinders in a bed of rocks leads to the increase of the thermal storage unit energy content and the enhancement of vertical thermal conductivity. Sharifi et al. [43] numerically investigated the melting of a sodium nitrate ($NaNO_3$, T_m = 307 °C) enclosed by a cylindrical container which is heated by a vertical heat pipe. The effectiveness of the HP-assisted system was evaluated by comparing it to an equivalent unit with an isothermal surface, a rod and a tube. Also, the effects of heating orientation, heat pipe length and diameter were considered. The results showed that the melting rate is enhanced with the increase of both HP length and diameter. Furthermore, it was shown that the melting rate associated with HP-assisted system is considerably higher than that of a system with rod or tube. Nithyanandam and Pitchumani [44] employed a three-dimensional numerical procedure to analyze the melting process of potassium nitrate in a shell and tube LHTES assisted with heat pipes. They studied the effects of number and orientation of the heat pipes on the system effectiveness.

Recently, Shabgard et al. [45] developed a two-dimensional model to study a HP-assisted LHTES system with sodium chloride (NaCl, T_m = 800 °C) PCM. They used a conduction-controlled model for melting in which the effect of natural convection within the molten PCM was neglected. Also, instead of considering conjugate heat transfer in fins and PCM, they assumed a homogenous anisotropic

PCM with effective thermophysical properties. The effective properties were calculated based on volume fraction of the fins, defined as the fin volume to the total volume of the fin-PCM system. It was found that the PCM acts as a capacitor which damps the temporal variations of input heat flux and makes thermal power output relatively smooth. In addition, it was shown that the number of HPs has a great influence on the transient response of LHTES system.

As can be seen that majority of the studies were focused on low melting temperature PCMs and only a limited number of numerical studies have been dedicated to the simulation of high temperature LHTES systems. In these analyses, the startup process was ignored assuming uniform initial temperature distribution of PCM very close to its melting temperature. However, in reality the startup process from ambient temperature could lead to non-uniformed temperature distribution of the PCM when the melting begins. In the present work, the charging process of a LHTES system with PCM enclosed by a square container is studied. The charging process of the unit is conducted by imposing constant heat flux at the base wall of the container. The system charging process starts from ambient temperature. Based on authors' past experience, charging from room temperature may result in system overheating specially in the base wall where high heat flux is applied. A single or multiple heat pipes with fins mounted on their condenser section is embedded in the PCM to alleviate this issue. The discharging process is not considered in this study, because overheating is not a concern during the discharging process. Discharging process has its own technical challenges, such as PCM rapid solidification around heat pipes resulting in increased temperature drop and reduced heat transfer. The results for the discharging process will be reported in our future papers.

The objective of this study is to numerically investigate the effects of heat pipes spacing and geometrical features of the fins attached to them, as well as the influence of natural convection heat transfer on the charging process of LHTES system starting from room temperature.

2. Physical model

Only the charging process of a LHTES system is investigated in this study. The physical geometry of the LHTES system is illustrated in Fig. 1. Three sets of models containing single or multiple heat pipes are analyzed. The heat pipes are composed of evaporator (heat receiver) and condenser (heat rejecter) sections. Uniform heat flux is applied to the heat pipe evaporator which covers the bottom surface of PCM container. The condenser sections of heat pipes have Nickel fins attached for better heat spread through the PCM. The container length is L = 254 mm. The thickness of heat pipe evaporator is t_r = 10 mm and the length and thickness of the heat pipe condenser are L_{hp} = 250 mm and t_{hp} = 10 mm, respectively. The geometric dimensions of three cases are provided in Table 1.

The entire system is initially at ambient temperature (T_{in} = 300 K) and the charging mode starts at τ = 0 s at constant heat flux of 40 kW/m^2 to the heat pipe evaporator. All other walls are considered to be adiabatic during charging process. The thermophysical properties of PCM, fins and heat pipes are shown in Table 2.

Following assumptions are made in the numerical modeling. The melting process is modeled using enthalpy-porosity technique. The PCM properties are assumed to be constant and equal for both solid and liquid phases. The molten PCM is considered Newtonian and Boussinesq fluid. Flow within the molten PCM is incompressible and laminar. Radiation heat transfer is neglected. The volume change during melting process is disregarded. Also, the motion of solid PCM is neglected during the phase change. In addition, thermal contact resistances are ignored at the interfaces.

3. Governing equations

Governing equations are given as follows:

3.1. PCM

Continuity equation:

$$\frac{\partial(\rho u)}{\partial x}+\frac{\partial(\rho v)}{\partial y}=0 \tag{1}$$

where ρ is the PCM density; u and v are velocities in x and y directions, respectively.

x-momentum:

$$\frac{\partial(\rho u)}{\partial \tau}+\frac{\partial(\rho u u)}{\partial x}+\frac{\partial(\rho u v)}{\partial y}=-\frac{\partial P}{\partial x}+\frac{\partial}{\partial x}\left(\mu\frac{\partial u}{\partial x}\right)+\frac{\partial}{\partial y}\left(\mu\frac{\partial u}{\partial y}\right)+S_x \tag{2}$$

y-momentum:

$$\frac{\partial(\rho v)}{\partial \tau}+\frac{\partial(\rho u v)}{\partial x}+\frac{\partial(\rho v v)}{\partial y}=-\frac{\partial P}{\partial y}+\frac{\partial}{\partial x}\left(\mu\frac{\partial v}{\partial x}\right)+\frac{\partial}{\partial y}\left(\mu\frac{\partial v}{\partial y}\right)+\rho g\beta(T-T_m)+S_y \tag{3}$$

where μ is the PCM viscosity. The enthalpy-porosity approach treats the mushy zone as a porous medium. The porosity in each element is assumed to be equal to the liquid fraction of that element. The

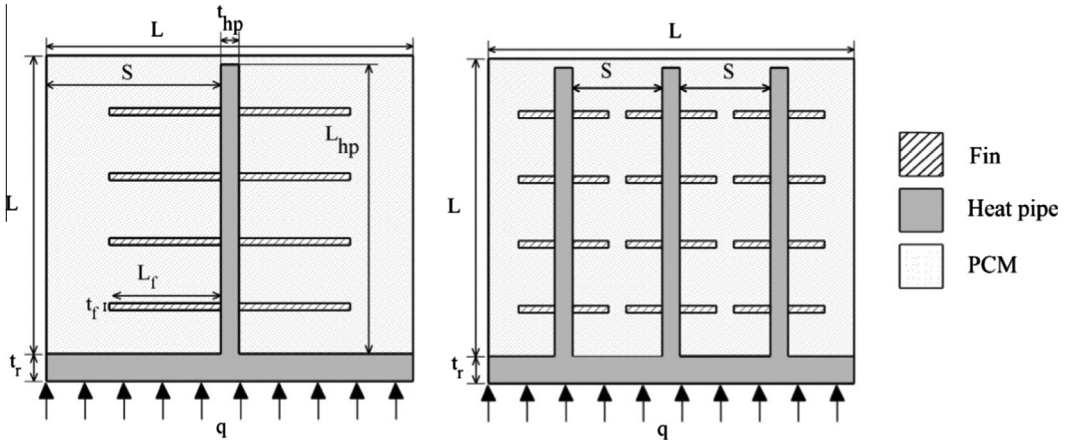

Fig. 1. Schematics of the LHTES units; with one central heat pipe (left) and with three heat pipes (right).

Table 1
Dimensions of the cases studied.

Model	Number of fins (N)	Spacing (S), mm	Fin thickness (t_f), mm	Fin length (L_f), mm
1 HP	10	122	2	80, 100, 120
	20		1	
3HP	10	74	2	15, 25, 35
	20		1	
5HP	10	41	2	10, 15, 19
	20		1	

Table 2
Thermophysical properties of the LHTES system components.

Properties	PCM (KNO3)[56,57]	Fins (Nickel)	Heat pipe
Melting point, T_m (K)	608	–	–
Latent heat of fusion, h_{sl} (kJ/kg)	95	–	–
Density, ρ (kg/m^3)	2109	8900	8978
Specific heat, c_p (J/kg K)	953	460.6	381
Thermal conductivity, k (W/m K)	0.5	91.74	3.8×10^4
Liquid viscosity, μ (Pa s)	2.59×10^{-3}	–	–
Thermal expansion coefficient, β (1/K)	2×10^{-4}	–	–

momentum sink terms S_x and S_y due to the reduced porosity in the mushy zone are defined as [46,47]:

$$S_x = -\frac{(1-f_l)^2}{f_l^3+\varepsilon} A_{mush}(u-u_p) \tag{4}$$

$$S_y = -\frac{(1-f_l)^2}{f_l^3+\varepsilon} A_{mush}(v-v_p) \tag{5}$$

where f_l is the liquid volume fraction and is defined based on the PCM temperature:

$$\begin{aligned} &f_l = 0 \quad \text{if} \quad T < T_{solidus} \\ &f_l = 1 \quad \text{if} \quad T > T_{liquidus} \\ &f_l = \frac{T - T_{solidus}}{T_{liquidus} - T_{solidus}} \quad \text{if} \quad T_{solidus} < T < T_{liquidus} \end{aligned} \tag{6}$$

ε is a small number to prevent division by zero and A_{mush} is the mushy zone constant which measures the amplitude of damping; the higher it is, the steeper is the material velocity transition to zero when solidifies. Different values of mushy zone constant ranged from 10^3 to 10^{10} were reported in previous numerical studies [47–49]. In the present work, A_{mush} is assigned to a value of 2.5×10^6 which shows the best consistency with previous experimental works. However, the authors believe that even more accurate predictions can be achieved by considering non-constant mushy zone parameter which can be estimated based on the liquid fraction of PCM during the phase change process. The validity of this hypothesis needs further investigation and will be carried out in near future. Also, u_p and v_p are the pull velocities which pull solidified material out of domain. But, their effects are neglected in the present work [46].

Energy equation:

$$\frac{\partial(\rho H)}{\partial \tau} + \frac{\partial(\rho u H)}{\partial x} + \frac{\partial(\rho v H)}{\partial y} = \frac{\partial}{\partial x}\left(k\frac{\partial T}{\partial x}\right) + \frac{\partial}{\partial y}\left(k\frac{\partial T}{\partial y}\right) \tag{7}$$

where, k is thermal conductivity of the PCM and H is the enthalpy of PCM. Enthalpy is computed as the sum of sensible enthalpy, h, and the latent heat, ΔH:

$$H = h + \Delta H \tag{8}$$

where

$$h = h_{ref} + \int_{T_{ref}}^{T} c_p dT \tag{9}$$

h_{ref} is the reference enthalpy, T_{ref} is the reference temperature and c_P is the specific heat at constant pressure [46]. The latent heat is written in terms of the latent heat of fusion of the PCM, h_{sl}:

$$\Delta H = f_l h_{sl} \tag{10}$$

The latent heat varies between zero (for solid PCM) and h_{sl} (for liquid PCM).

3.2. Heat pipe

Heat pipes are capable of transferring heat at much higher rate than solid conductors such as aluminum or copper by taking advantages of liquid and vapor transition. However, it is difficult to simulate all the physical phenomena inside heat pipes. Therefore, usually they are considered as a very high thermal conductive element within an energy storage system in numerical modeling. Legierski et al. [50] reported the maximum effective thermal conductivity of 30 kW/m K for a horizontal heat pipe with water as working fluid. While, the higher values (up to 50 kW/m K) are recommended by Thyrum [51] at different operating conditions. El-Nasr and El-Haggar [52] reported values up to 100 kW/m K for different configurations and working temperatures based on their experiments. Moreover, Faghri [29] described heat pipe as a device with thermal conductivity up to 90 times greater than a copper rod with the same size.

As discussed above, majority of the works done so far treated heat pipes as elements with constant, high thermal conductivity. A very few studies considered heat pipes as time dependent devices but did not provide any data for time dependent thermal conductivity. In the present study, heat pipe is modeled as an element with high effective, constant thermal conductivity k_{eff}. We are working on the modeling of transient heat pipes which will provide time dependent HP thermal conductivity data and will be employed in our future works.

The energy equation for the heat pipe is:

$$(\rho c_p)_{eff}\frac{\partial T}{\partial \tau} = k_{eff}\left[\frac{\partial^2 T}{\partial x^2} + \frac{\partial^2 T}{\partial y^2}\right] \tag{11}$$

Table 3
The grid and time-step independence test results.

Time step (s)		Grid 1 ($N_x \times N_y$)	Grid 2 ($N_x \times N_y$)	Grid 3 ($N_x \times N_y$)
$\Delta\tau_1$	$\Delta\tau_2$	50×100 Charging time (s)	70×140	100×200
10	0.05	6774	–	–
5	0.02	6851	6887	–
1	0.01	6907	6920	6924
1	0.005	6929	6926	6921

3.3. Fins

The energy equation of the fin is:

$$(\rho c_p)_f \frac{\partial T}{\partial \tau} = k_f \left[\frac{\partial^2 T}{\partial x^2} + \frac{\partial^2 T}{\partial y^2}\right] \quad (12)$$

4. Numerical method and validation

The commercial CFD package of ANSYS FLUENT14.0 was employed to solve the governing equations. ANSYS design modeler was used to create the physical model. Due to the symmetry of flow and temperature fields relative to y axis, half of the physical domain was modeled. The structured uniform grid was applied to discretize the computational domain. The PRESSURE BASED method within FLUENT 14.0 was utilized to solve PCM momentum equations by applying SIMPLE scheme for velocity–pressure coupling. Second Order Upwind differencing method was used for the discretization of convective terms in momentum and energy equations. Also, Standard scheme was adopted for pressure interpolation at the cell-faces. The further details about the numerical methods can be found in reference [53].

In order to improve the convergence stability, the under-relaxation factors of 0.5, 0.3 and 0.9 were considered for the momentum, pressure and liquid fraction, respectively.

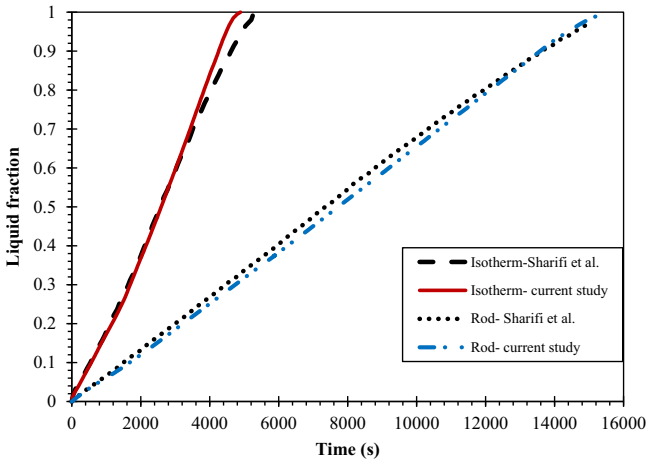

Fig. 3. Comparison of liquid fraction history with the work of Sharifi et al. [43].

Convergence residual values of 10^{-4}, 10^{-8} and 10^{-10} were set for continuity, momentum (x and y velocities) and energy equations, respectively. In each time step, the convergence criteria were achieved after 1000–2000 iterations.

The results of grid and time step independence test are shown in Table 3 for the case with 1 HP. After conducting the test, a uniform grid with 70 elements in x-direction and 140 elements in y-direction for the given dimensions was found sufficient for all the computations. Time step of 1 s was used in solid PCM state, while this value was reduced to 0.01 s after the start of phase change. Additional time step refinement did not enhance the accuracy of the computations. Simulations were carried out by a computer with 3.4 GHz Intel processors and 8 GB RAM. The average CPU time of one week was required for the simulation of a complete charging process.

To evaluate the validity of the numerical model, the obtained results from the present study were compared to those reported by previous experimental and numerical studies. Fig. 2 shows the melt front locations at various times of current study, experimental

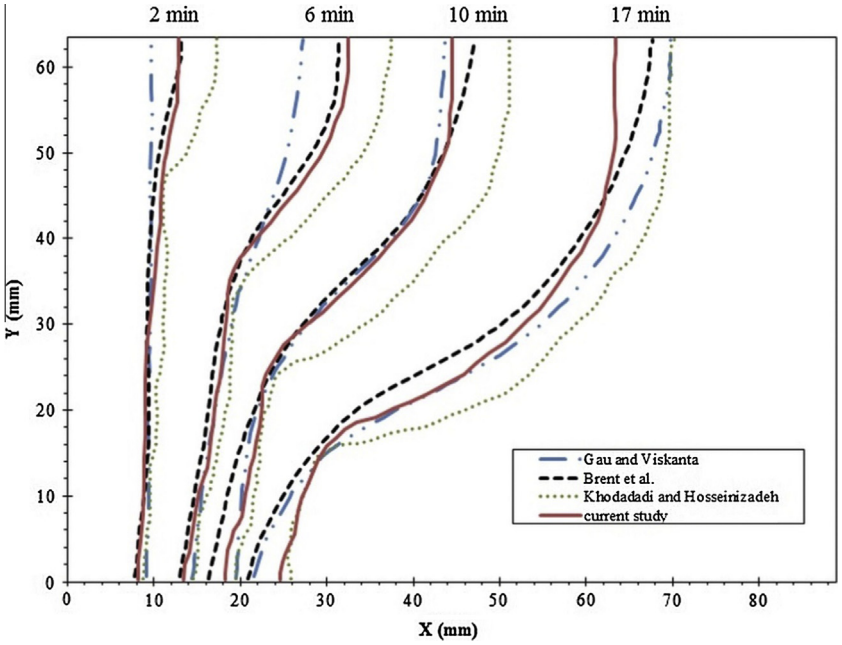

Fig. 2. Melt front locations at different times: Comparison among the experimental measurement of Gau and Viskanta [54], numerical prediction of Brent et al. [55], current study and Khodadadi and Hosseinizadeh [16].

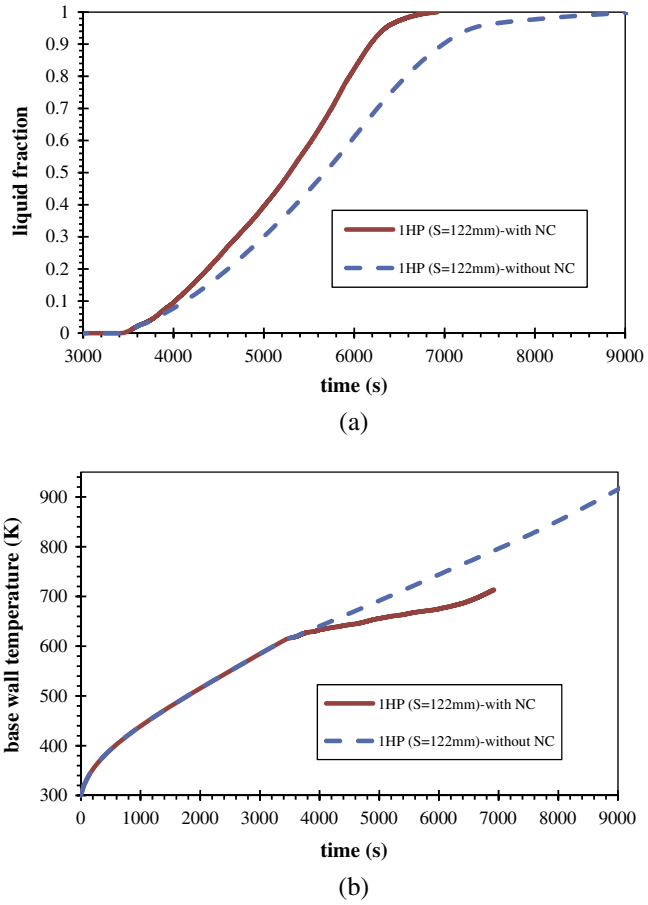

Fig. 4. (a) Liquid fraction history, and (b) variation of base wall temperature for the case with 1 HP (S = 122 mm).

data by Gau and Viskanta [54], and numerical results by Brent et al. [55] and Khodadadi and Hosseinizadeh [16]. Very good agreement exists between the results of current study and previous works. The small difference between the experimental data and current numerical results may be caused by three-dimensional characteristics of flow within the liquid PCM as well as the variations in PCM properties. The discrepancy between the present study and other numerical models is likely due to the difference in the details of numerical methods and parameters such as mushy zone constant which strongly affects the results.

Also, the predictions for the melting of sodium nitrate ($NaNO_3$) PCM computed by present method are compared to the results reported by Sharifi et al. [43]. The dimensional details of the model and the physical properties of sodium nitrate PCM can be found in [43]. The histories of PCM liquid fraction are compared to the work of Sharifi et al. [43] where melting was induced by an isothermal surface and a hot metal rod, Fig. 3. They are in good agreement. The source of the minor discrepancy between the present study and Sharifi's data is resulted from the difference of the numerical approaches. Sharifi used a temperature transforming model while this study uses enthalpy-porosity technique to simulate the phase change process.

5. Results and discussion

5.1. Effects of natural convection

To understand the role of natural convection heat transfer mechanism in the melting process, the liquid fraction of PCM as well as base wall temperature histories were studied for the cases with one central heat pipe with or without consideration of natural convection effects. Fig. 4a shows the transient behavior of PCM liquid fraction for the cases studied. As expected, melting process starts at the same time for both cases. At the early stage, similar liquid fractions are obtained for both cases due to the fact that there exists only a thin layer of molten PCM and weak natural convection circulations. However, as the thickness of liquid layer increases the effect of natural convection becomes significant, resulting in increased heat transfer rate to the PCM and higher amount of liquid fraction for the case with natural convection. As can be seen, including the effect of natural convection accelerates the melting process of the PCM; hence reduces the total charging time by approximately 30%.

Fig. 4b depicts the temporal temperature of base wall which is exposed to the constant heat flux during the charging process. The wall is initially at 300 K for both cases. As the charging continues (before the start of PCM melting), both cases result in exactly the same temperature, since the heat transfer process is only governed by conduction mechanism. After the start of PCM melting, natural convection reduces the thermal resistance between the base wall

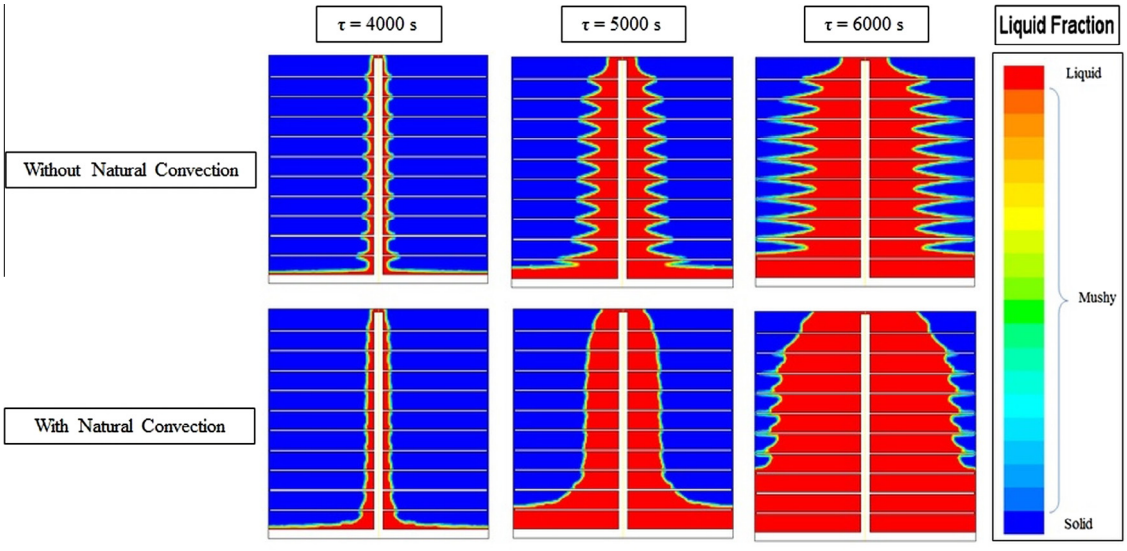

Fig. 5. Contours of the volume fraction of the PCM at different times.

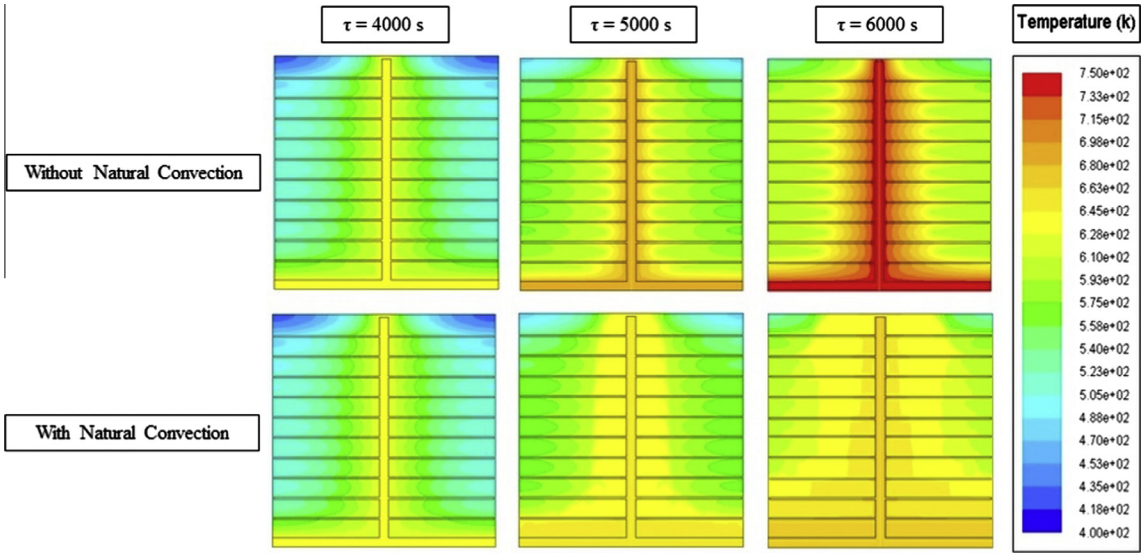

Fig. 6. Temperature distributions for the case with 1 HP (S = 122 mm) at various times.

and melt front causing a considerable reduction in the base wall temperature in comparison to conduction only case. Similar behavior has been reported by Shabgard et al. [38].

The liquid–solid interface contours at three different times are illustrated in Fig. 5 for the cases with and without considering the effect of natural convection. For the case without natural convection, the melting occurs at the proximity of the fins producing sharp edged melt fronts. While, by taking natural convection effect into account, the liquid–solid interface is flattened and moves faster.

Temperature distribution of the system is shown in Fig. 6 for the cases with and without natural convection at three distinct times. At the beginning of the PCM phase change, similar temperature patterns are observed for both cases due to the weak effect of natural convection, so that the heat transfer is dominantly controlled by conduction mechanism. As heating continues and molten PCM region extends, the natural convection effect is reinforced. The increased natural convection results in more uniform temperature distribution in molten PCM near the hot walls and reduces the temperature of base wall, preventing the system from overheating of container material.

5.2. Effects of heat pipe spacing (number of HPs)

The variations of PCM liquid volume fraction, as well as the temporal variations of base wall temperature for different heat pipe spacing are shown in Fig. 7a and b. As can be seen in Fig. 7a, PCM melting starts earlier in the LHTES with bigger HP spacing (lower number of HPs). It is due to higher thermal resistance associated with lower numbers of HPs (bigger HP spacing). The higher thermal resistance, at the same input heat flux results in higher temperature difference between base wall and PCM and higher temperature in the PCM close to the base wall since the most of thermal energy is transferred and stored in the PCM near the wall. For the cases with smaller HP spacing, lower temperature is obtained adjacent to the wall; and the temperature distribution is more uniform in the entire PCM because of better heat spread resulted from higher numbers of HPs (smaller HP spacing). Melting starts later near the wall for smaller HP spacing (S = 74 and 41 mm), however, it proceeds much faster in comparison to the larger spacing (S = 122 mm). As charging continues, these higher melting rates yield higher liquid fractions for the smaller spacing cases, indicating more uniformed energy storage. Consequently,

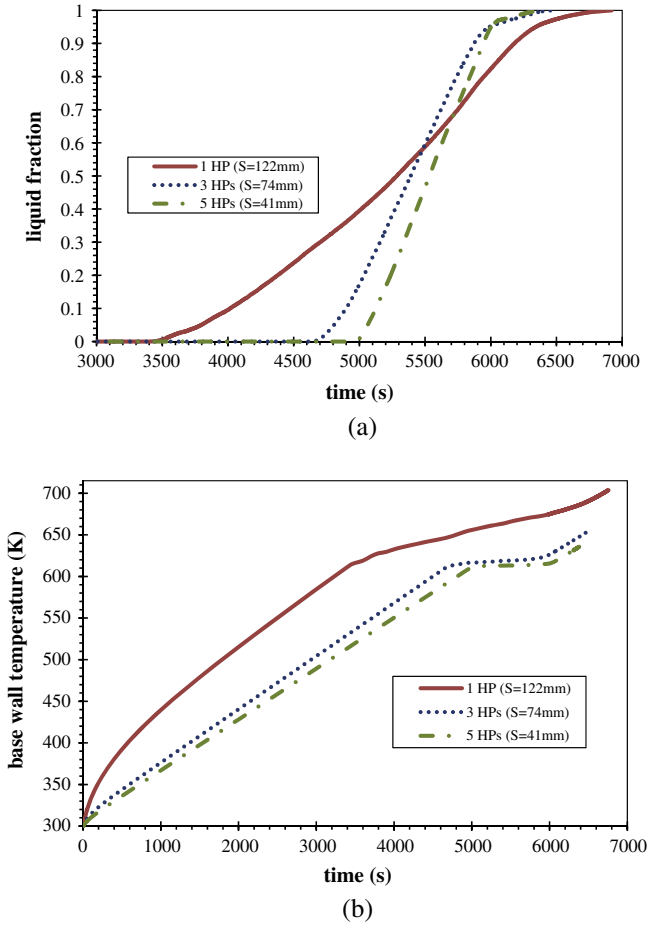

Fig. 7. (a) Liquid fraction history and, (b) temporal base wall temperature associated with different heat pipe spacing.

decreasing the HP spacing leads to faster charging. Generally, increasing the number of HPs from 1 to 3 results in around 10% reduction in LHTES system charging time. There is not much a difference between the LHTES with 3 HPs and 5 HPs; the benefits of adding more HPs diminish.

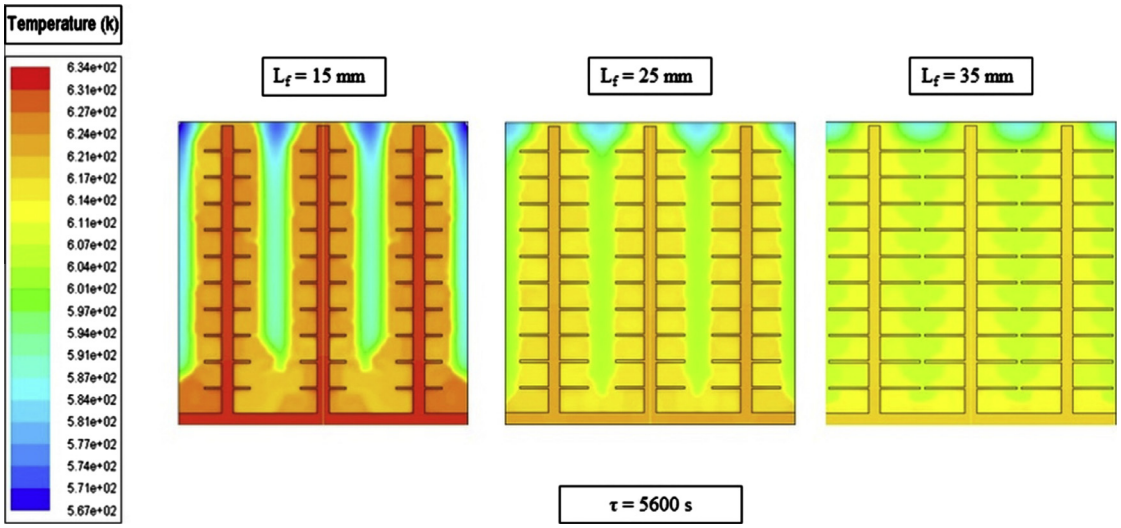

Fig. 8. Temperature distributions for the cases with 3 HPs (S = 74 mm) with different fin lengths.

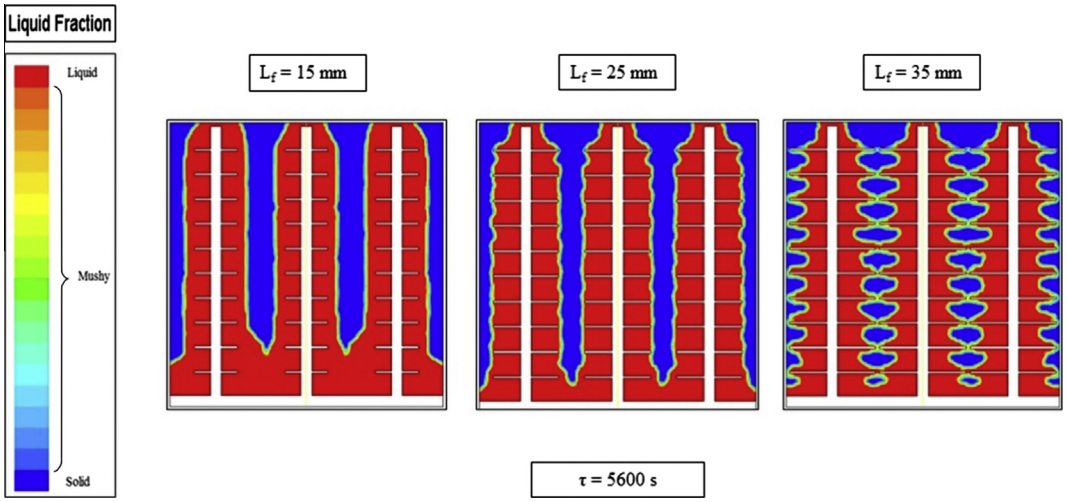

Fig. 9. Contours of the volume fraction of the PCM for the cases with 3 HPs (S = 74 mm) with different fin lengths.

Fig. 7b shows the base wall temperature versus time for different HP spacing. Due to higher thermal resistance associated with larger HP spacing, higher base wall temperatures are obtained for these cases during the system charging. In all cases, the slope of base wall temperature decreases right after the start of PCM phase change, because the heat storage mechanism changes from sensible heat to latent heat. Also, as the melting process progresses, more PCM liquid is formed adjacent to the base wall and HP surfaces and natural convection starts, which enhances the heat transfer from hot walls to PCM, leading to a slower base wall temperature growth. The slope change in Fig. 7b is more profound for the smaller HP spacing and the base wall temperature is nearly constant at the early stage of salt melting. This behavior can be explained by noting that using higher numbers of heat pipes provides better heat spread. Consequently, the input thermal energy is transferred to the PCM away from the base wall via HPs efficiently. This energy is used to heat and melt PCM instead of accumulating near the base wall.

In the final stages of charging process, Fig. 7a and b, LHTES systems with smaller HP spacing provide higher PCM liquid fraction and lower base wall temperature. Therefore, increasing the numbers of HPs results in the enhancement of heat transfer to the PCM with lower temperature difference between the base wall and solid part of the PCM. Also, by comparing the PCM liquid fraction and base wall temperature histories for different HP spacing, it can be seen that the systems with 3 and 5 HPs (S = 74 and 41 mm) provide higher performance in comparison to the one with 1 HP (S = 122 mm). There is not a much difference between the results of 3 HPs and 5 HPs. Thus, the LHTES assisted by 3 HPs seems to be an optimum spacing configuration for the given geometry since the manufacturing cost of the system is reduced by employing less number of heat pipes and the heat storage capacity of the system is increased as more PCM mass can be added to the system by eliminating those two heat pipes.

5.3. Effects of fin length

Three different cases were computed to study the effects of fins length on thermal performance of the LHTES system. Each case contains 3 heat pipes with 10 fins attached to each heat pipe. Fins lengths are 15, 25 and 35 mm, respectively. Figs. 8 and 9 illustrate the temperature distributions inside the PCM container and the contours of solid–liquid interface for each case at τ = 5600 s. Also, Fig. 10a displays the liquid fraction histories of three cases. Base

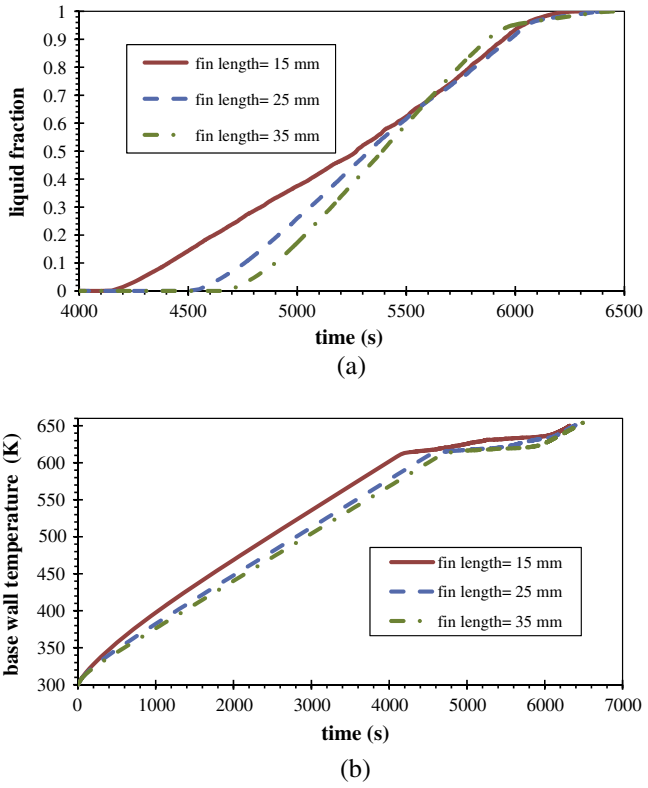

Fig. 10. (a) Liquid fraction history and, (b) base wall temperature for the case with 3 HPs (S = 74 mm) with different fin lengths.

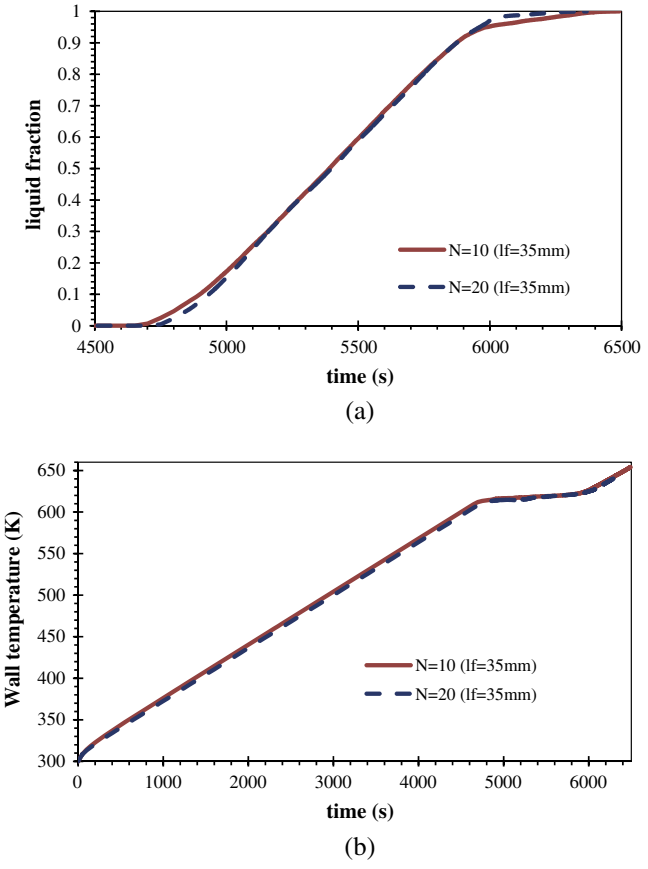

Fig. 11. (a) Liquid fraction history and, (b) temporal base wall temperature for the case with 3 HPs (S = 74 mm) for different number of fins.

wall temperature for these cases is depicted in Fig. 10b. From Fig. 10a, it can be seen that at τ = 5600 s, all three cases have approximately the same amount of PCM liquid fraction. Longer fins provide higher interfacial surface areas between the fins and the PCM, therefore higher heat transfer from hot walls to PCM, which results in more uniformed temperature distribution within the PCM and lower base wall temperatures. The temperature difference between the solid PCM and heat pipes surface decreases with the increase of fin length due to better heat spread associated with the longer fins.

Melting starts earlier in the cases with shorter fins, Fig. 10a, because majority of the thermal energy is transferred to PCM close to base wall instead of spreading out. This is due to higher thermal resistance associated with the systems with shorter fins. This higher thermal resistance also attributes to the higher base wall temperature during the charging process as shown in Fig. 10b. Although the cases with longer fins (L_f = 25 and 35 mm) show higher melting rates after the start of melting, the total charging time is shorter for the system with shortest fins. This phenomenon can be attributed to the blockage of molten PCM flow between fins and weakened natural convection related to longer fins.

5.4. Effects of number of the fins

To investigate the influence of fin number on charging process of the LHTES system, two cases with the same HP spacing of 74 mm (3 HPs) and different numbers of fins (N = 10 and 20) attached to each heat pipe are studied. The fins have the same length in both cases (L_f = 35 mm) but different thickness (t_f = 2 mm for N = 10 and t_f = 1 mm for N = 20). Therefore, both LHTES systems contain the same amount of fin material (Nickel) and PCM.

As the number of fins increases, the interfacial surface area between the fins and PCM increases, leading to lower thermal resistance of the system. It is evidenced by delayed start of melting and lower base wall temperature for the case with 20 fins, as shown in Fig. 11a and b. However, higher number of fins restricts the motion of molten PCM resulting in a strong suppression of natural convection within the molten salt. As the melting progresses, these two factors offset each other. As a result, the total charging time and base wall temperature variations at both fin numbers (N = 10 and 20) are almost the same.

6. Conclusions

The charging process of a finned heat pipe-assisted LHTES system with a high melting temperature PCM enclosed by a square container was simulated using a transient two-dimensional model. The effects of heat pipe spacing, fin length and numbers as well as the influence of natural convection on the performance of the system were studied. Numerical analysis showed that the natural convection has considerable effects on the melting process of the PCM. It accelerates the charging and reduces the total charging time by approximately 30%. Also, natural convection helps to yield more uniformed temperature distribution within the PCM and also lower the base wall temperature of the container, which prevents system overheating and material failure. It was found that heat pipe spacing also plays a key role in the enhancement of LHTES system performance. Increasing the number of HPs (decreasing the heat pipe spacing) leads to the increase of melting rate and the decrease of base wall temperature during the charging process. The geometry of the fins attached to the heat pipes plays an important role in the performance of the system. The increase of fin length resulted in the decrease of temperature difference within PCM, as well as lower base wall temperature. It was also shown that number of the fins does not affect the performance of the system significantly.

Acknowledgment

The authors gratefully appreciate the financial supports provided by Temple University.

References

[1] Sharma SD, Iwata T, Kitano H, Sagara K. Thermal performance of a solar cooker based on an evacuated tube solar collector with a PCM storage unit. Sol Energy 2005;78:416–26.
[2] Reyes A, Negrete D, Mahn A, Sepúlveda F. Design and evaluation of a heat exchanger that uses paraffin wax and recycled materials as solar energy accumulator. Energy Convers Manage 2014;88:391–8.
[3] Shatikian V, Ziskind G, Letan R. Numerical investigation of a PCM-based heat sink with internal fins: constant heat flux. Int J Heat Mass Transf 2008;51:1488–93.
[4] Yang Y-T, Wang Y-H. Numerical simulation of three-dimensional transient cooling application on a portable electronic device using phase change material. Int J Therm Sci 2012;51:155–62.
[5] Wang Y-H, Yang Y-T. Three-dimensional transient cooling simulations of a portable electronic device using PCM (phase change materials) in multi-fin heat sink. Energy 2011;36:5214–24.
[6] Bony J, Citherlet S. Numerical model and experimental validation of heat storage with phase change materials. Energy Build 2007;39:1065–72.
[7] Mazman M, Cabeza LF, Mehling H, Nogues M, Evliya H, Paksoy HÖ. Utilization of phase change materials in solar domestic hot water systems. Renewable Energy 2009;34:1639–43.
[8] Zukowski M. Mathematical modeling and numerical simulation of a short term thermal energy storage system using phase change material for heating applications. Energy Convers Manage 2007;48:155–65.
[9] Çakmak G, Yıldız C. The drying kinetics of seeded grape in solar dryer with PCM-based solar integrated collector. Food Bioprod Process 2011;89:103–8.
[10] Shalaby SM, Bek MA. Experimental investigation of a novel indirect solar dryer implementing PCM as energy storage medium. Energy Convers Manage 2014;83:1–8.
[11] Mosaffa AH, Infante Ferreira CA, Talati F, Rosen MA. Thermal performance of a multiple PCM thermal storage unit for free cooling. Energy Convers Manage 2013;67:1–7.
[12] Azzouz K, Leducq D, Gobin D. Performance enhancement of a household refrigerator by addition of latent heat storage. Int J Refrig 2008;31:892–901.
[13] Pandiyarajan V, Chinna Pandian M, Malan E, Velraj R, Seeniraj RV. Experimental investigation on heat recovery from diesel engine exhaust using finned shell and tube heat exchanger and thermal storage system. Appl Energy 2011;88:77–87.
[14] Arasu AV, Mujumdar AS. Numerical study on melting of paraffin wax with Al2O3 in a square enclosure. Int Commun Heat Mass Transfer 2012;39:8–16.
[15] Fukai J, Kanou M, Kodama Y, Miyatake O. Thermal conductivity enhancement of energy storage media using carbon fibers. Energy Convers Manage 2000;41:1543–56.
[16] Khodadadi JM, Hosseinizadeh SF. Nanoparticle-enhanced phase change materials (NEPCM) with great potential for improved thermal energy storage. Int Commun Heat Mass Transfer 2007;34:534–43.
[17] Hosseinizadeh SF, Darzi AAR, Tan FL. Numerical investigations of unconstrained melting of nano-enhanced phase change material (NEPCM) inside a spherical container. Int J Therm Sci 2012;51:77–83.
[18] Baby R, Balaji C. Experimental investigations on thermal performance enhancement and effect of orientation on porous matrix filled PCM based heat sink. Int Commun Heat Mass Transfer 2013;46:27–30.
[19] Hong S-T, Herling DR. Open-cell aluminum foams filled with phase change materials as compact heat sinks. Scripta Mater 2006;55:887–90.
[20] Zhao CY, Wu ZG. Heat transfer enhancement of high temperature thermal energy storage using metal foams and expanded graphite. Sol Energy Mater Sol Cells 2011;95:636–43.
[21] Kim T, France DM, Yu W, Zhao W, Singh D. Heat transfer analysis of a latent heat thermal energy storage system using graphite foam for concentrated solar power. Sol Energy 2014;103:438–47.
[22] Yang Z, Garimella SV. Melting of phase change materials with volume change in metal foams. J Heat Transfer 2010;132:062301.
[23] Almajali M, Lafdi K, Prodhomme PH. Effect of copper coating on infiltrated PCM/foam. Energy Convers Manage 2013;66:336–42.
[24] Thapa S, Chukwu S, Khaliq A, Weiss L. Fabrication and analysis of small-scale thermal energy storage with conductivity enhancement. Energy Convers Manage 2014;79:161–70.
[25] Sharifi N, Bergman TL, Faghri A. Enhancement of PCM melting in enclosures with horizontally-finned internal surfaces. Int J Heat Mass Transf 2011;54:4182–92.
[26] Lacroix M, Benmadda M. Numerical simulation of natural convection-dominated melting and solidification from a finned vertical wall. Numer Heat Transfer A: Appl 1997;31:71–86.
[27] Gharebaghi M, Sezai I. Enhancement of heat transfer in latent heat storage modules with internal fins. Numer Heat Transfer A: Appl 2007;53:749–65.
[28] Mat S, Al-Abidi AA, Sopian K, Sulaiman MY, Mohammad AT. Enhance heat transfer for PCM melting in triplex tube with internal–external fins. Energy Convers Manage 2013;74:223–36.
[29] Faghri A. Heat pipe science and technology. Taylor and Francis; 1995.
[30] Horbaniuc B, Popescu A, Dumitraşcu G. The correlation between the number of fins and the discharge time for a finned heat pipe latent heat storage system. Renewable Energy 1996;9:605–8.
[31] Horbaniuc B, Dumitrascu G, Popescu A. Mathematical models for the study of solidification within a longitudinally finned heat pipe latent heat thermal storage system. Energy Convers Manage 1999;40:1765–74.
[32] Liu Z, Wang Z, Ma C. An experimental study on heat transfer characteristics of heat pipe heat exchanger with latent heat storage. Part I: charging only and discharging only modes. Energy Convers Manage 2006;47:944–66.
[33] Liu Z, Wang Z, Ma C. An experimental study on the heat transfer characteristics of a heat pipe heat exchanger with latent heat storage. Part II: simultaneous charging/discharging modes. Energy Convers Manage 2006;47:967–91.
[34] Robak CW, Bergman TL, Faghri A. Enhancement of latent heat energy storage using embedded heat pipes. Int J Heat Mass Transf 2011;54:3476–84.
[35] Sharifi N, Bergman TL, Allen MJ, Faghri A. Melting and solidification enhancement using a combined heat pipe, foil approach. Int J Heat Mass Transf 2014;78:930–41.
[36] High Energy Advanced Thermal Storage (HEATS) Funding Opportunity Announcement. Advanced Research Projects Agency (ARPA-E), Department of Energy, DE-FOA-0000471 CFDA Number 81135; 2011.
[37] Qiu S, Galbraith R, White M. Phase change material thermal energy storage system design and optimization. In: ASME 2013 7th International Conference on Energy Sustainability, Minneapolis, Minnesota, USA; 2013.
[38] Shabgard H, Bergman TL, Sharifi N, Faghri A. High temperature latent heat thermal energy storage using heat pipes. Int J Heat Mass Transf 2010;53:2979–88.
[39] Nithyanandam K, Pitchumani R. Analysis and optimization of a latent thermal energy storage system with embedded heat pipes. Int J Heat Mass Transf 2011;54:4596–610.
[40] Jung EG, Boo JH. Thermal analytical model of latent thermal storage with heat pipe heat exchanger for concentrated solar power. Sol Energy 2014;102:318–32.
[41] Guo C, Zhang W. Numerical simulation and parametric study on new type of high temperature latent heat thermal energy storage system. Energy Convers Manage 2008;49:919–27.
[42] Okello D, Foong CW, Nydal OJ, Banda EJK. An experimental investigation on the combined use of phase change material and rock particles for high temperature (~350 °C) heat storage. Energy Convers Manage 2014;79:1–8.
[43] Sharifi N, Wang S, Bergman TL, Faghri A. Heat pipe-assisted melting of a phase change material. Int J Heat Mass Transf 2012;55:3458–69.
[44] Nithyanandam K, Pitchumani R. Computational studies on a latent thermal energy storage system with integral heat pipes for concentrating solar power. Appl Energy 2013;103:400–15.
[45] Shabgard H, Faghri A, Bergman TL, Andraka CE. Numerical simulation of heat pipe-assisted latent heat thermal energy storage unit for dish-Stirling systems. J Sol Energy Eng 2013;136:021025.
[46] FLUENT 6.3 User's Guide. Fluent Inc., Lebanon; 2006.
[47] Voller VR, Prakash C. A fixed grid numerical modelling methodology for convection-diffusion mushy region phase-change problems. Int J Heat Mass Transf 1987;30:1709–19.
[48] Gong Z-X, Devahastin S, Mujumdar AS. Enhanced heat transfer in free convection-dominated melting in a rectangular cavity with an isothermal vertical wall. Appl Therm Eng 1999;19:1237–51.
[49] Shmueli H, Ziskind G, Letan R. Melting in a vertical cylindrical tube: numerical investigation and comparison with experiments. Int J Heat Mass Transf 2010;53:4082–91.
[50] Legierski J, Więcek B, de Mey G. Measurements and simulations of transient characteristics of heat pipes. Microelectron Reliab 2006;46:109–15.
[51] Thyrum G. Critical aspects of modeling heat pipe assisted heat sinks <www.thermacore.com>.
[52] El-Nasr AA, El-Haggar SM. Effective thermal conductivity of heat pipes. Heat Mass Transf 1996;32:97–101.
[53] Patankar SV. Numerical heat transfer and fluid flow. New York: McGraw-Hill; 1980.
[54] Gau C, Viskanta R. Melting and solidification of a pure metal on a vertical wall. J Heat Transfer 1986;108:174–81.
[55] Brent AD, Voller VR, Reid KJ. Enthalpy-porosity technique for modeling convection-diffusion phase change: application to the melting of a pure metal. Numer Heat Transf 1988;13:297–318.
[56] Michels H, Pitz-Paal R. Cascaded latent heat storage for parabolic trough solar power plants. Sol Energy 2007;81:829–37.
[57] Lança M, Lourenço M, Santos F, Nunes V, de Castro CN. Viscosity of molten potassium nitrate. High Temp – High Pressures 2001;33:427–34.